Eleventh International Conference on the Bearing Capacity of Roads, Railways and Airfields, Volume 2 – Hoff, Mork & Saba (eds)

Modeling the loading behavior of railway structure under static load using a verified 3D finite element model

M. Peltomäki, P. Kolisoja & H. Luomala
Research Centre Terra, Tampere University, Tampere, Finland

ABSTRACT: When trying to optimize the life-cycle behavior of railway structures it is important to identify the main deformation factors of the structure and to understand the influence mechanisms behind these. Due to the complex behavior of railway structures, powerful numerical tools are needed to get realistic simulation results. Therefore, the focus of this study has been to create a three-dimensional finite element model to simulate the loading behavior of railway structures under static load using non-linear material models. The model is verified using measured field data from heavily instrumented test structures. The calculations mainly focus on the behavior of railway embankments of different subgrade stiffness and axel load levels. It is shown that subgrade stiffness seems to have a major role on the behavior of railway structures, whereas the influence of the axel load seems to be fairly linear.

Keywords: FEM, railway, verification, modeling

1 INTRODUCTION

To optimize the technical performance of a track structure, it is important to recognize the factors influencing the loading behavior of the structure and to understand the underlying mechanics behind these. The use of numerical simulation tools makes it possible not only to study arbitrary structures, but also to analyze the behavior of different structures at a detailed level. However, to ensure the validity of the calculated results, the importance of model verification is emphasized when a theoretical approach is used.

Historically, Winkler's classical BOEF theory (Beam on Elastic Foundation) presented in 1867, can be considered as a starting point for modeling the loading behavior of a track structure. Based on Winkler's work, Hetényi created one of the earliest mathematical models of a ballasted railway track in 1946 to describe the deflection behavior of a rail on an elastic foundation. Later in the 1970s, various structural modeling software based on multilayer theory (e.g., GEOTRACK, ILLITRACK) started to become more common (Selig & Waters 1994; Robnett et al. 1975).

With the increase in the computing power of computers and the number of suitable modeling software, the element method has now become one of the key numerical tools in railway structure research and various 3D element method-based calculation models have been presented by different researchers. For example, Gallego et al. (2011) found that subgrade stiffness plays a key role in the overall stiffness of the structure - a similar observation has been made by Sowmiya et al. (2010) and Ganesh Babu & Sujatha (2010). In turn, Kalliainen et al. (2016) conducted a parametric study using nonlinear material models and found that the subgrade stiffness, structural layers thickness, and material properties, are the most significant factors affecting the load carrying capacity of a railway track. Also, detailed 3D FE-models

DOI: 10.1201/9781003222897-48

have been used to analyze the internal stress distribution in the structure (e.g., Powrie et al. (2007), Varadas et al. (2016)). Alongside static models, some researchers have also used dynamic models to estimate the loading effects of high-speed trains (e.g., Shahraki et al. 2014, Sayeed (2016)).

However, most existing models are based on simple linear elastic theory, in which the stress-dependency of strength and stiffness characteristic of granular materials is not considered. Also, the verification of the models could be considered deficient in some respects. Therefore, the aim of this study has been to create and verify a non-linear 3D FEM model to describe the stress-strain response of a railway structure. The model has been created using Plaxis 3D software (version 2017) and the verification uses versatile field measurement data from two heavily instrumented test structures.

2 MATERIAL MODELS AND CALCULATION PHASES

In the modeling method used, the calculation includes two phases; in the first phase, the model calculates the displacement and stress field due to its own weight for the structure. Then, in the second and actual calculation phase, the external load is activated, and the final results are calculated. The basic idea is that the model is parameterized in such a way that its primary static loading behavior corresponds to the resilient behavior of the real structure, which is hardened under several thousands of load cycles. However, mathematically the behavior of the model is plastic, so such an approach is valid only to describe the stress-strain response caused by a single load cycle. In the model, the isotopically hardening Hardening Soil material model (HS-model) has been used for the granular structural layers – The HS-model has also been used in many previous ballasted track-related studies (e.g. Indraratna & Nimbaikar 2013, Shahraki et al. 2014). In the HS-model, material stiffness depends on the minor principal stress σ_3 and in primary loading stiffness corresponds to the secant modulus E_{50} (Plaxis 2017):

$$E_{50} = E_{50\,ref.} \left(\frac{c' \cdot \coth \varphi + \sigma_3}{c' \cdot \coth \varphi + \sigma_0} \right)^m \tag{1}$$

where $E_{50\,ref.}$ is the reference modulus, m is the stiffness exponent, σ_0 is the reference pressure used in the calculation (= 100 kPa), φ is the friction angle and c' is the cohesion (Plaxis 2017). In practice, the secant modulus determines the secant line slope that intersects the stress-strain curve through a point corresponding to 50% of the failure stress. The basic idea of the formulation of the HS-model is the hyperbolic relationship between primary strain and deviatoric stress in primary triaxial loading Hence, in a standard drained triaxial test, the relationship between primary strain ε_1 and stress state can be described by using the equation 2:

$$\varepsilon_1 = -\frac{2 - R_f}{2E_{50}} \frac{q}{1 - R_f q / q_f} \tag{2}$$

where q_f is the deviator stress corresponding to the failure state. In its original application, parameter R_f determines the shape of the yield curve at the plastic state and it can have values between 0 and 1. For natural sands, R_f has been found to be about 0.9 during virgin loading. However, in this study R_f describes the shape of the loading side of the hysteresis loop of already hardened soil material, and therefore the used values are slightly smaller than usual.

For the subsoil and superstructure components a linear elastic material model has been used, in which case the relationship between the stress and strains can be directly described by the elastic modulus E and Poisson's ration v of the material (Plaxis 2017). The material model of subsoil layers has been deliberately kept as simple as possible, allowing an unambiguous assessment of the effects of subsoil conditions in terms of the stress-strain behavior of the upper railway structure.

3 CALCULATION PARAMETERS

3.1 *Rails, sleepers, and interfaces*

In the created calculation model, the rails are modelled using one-dimensional beam elements and the calculation parameters used correspond to the 60E1 rail profile (SFS-EN 13674-1:2011); therefore value 210 GPa has been used as the modulus of elasticity of the rail steel, the rail cross section area is 0,00767 m^2 and the second moments of cross section area are $3.055 \cdot 10^{-5}$ m^4 for the vertical bending and $5.120 \cdot 10^{-6}$ m^4 for the horizontal bending.

The geometry of the modeled sleeper is based on the geometry of the B97 concrete sleeper with certain simplifications. The sleeper is modeled as a linear elastic material with an elastic modulus of 40 GPa and a Poisson's ratio of 0.15. In order for the sleeper to be able to move freely, all sides are separated from the surrounding ballast layer by interface elements. A contact factor of 0.01 has been used for the interface elements of the sleeper sides, whereby the shear strength and stiffness between sleeper and ballast is only one percent of the strength and stiffness of the surrounding ballast material - a more detailed mathematical description of the interface elements can be found in Plaxis (2017 b).

On flexible subsoils, the sleeper distributes most of its load through its ends when the underlying structure bends under the stiff sleeper. However, in this case, the deformation caused by the number of load cycles is mainly concentrated in the ends of the sleeper, causing a change in the sleeper support. To consider changing the support situation under train traffic, the interface elements between the sleeper and the underlying ballast layer are divided into several parts, in which case uneven support can be taken into account by changing the interface contact factors. Based on calculations, the contact factor distribution 0.33, 0.5 and 0.65 at the bottom of the sleeper (direction from the end of the sleeper to the center) proved to be a very good option. In this case, most of the load is transmitted directly through the contact area below the rail, without the discontinuous interface distribution causing unrealistically large node-specific load concentrations at the edges of the different interface areas.

3.2 *Ballast-layer and substructure*

As mentioned above, the ballast layer and substructure have been modeled using the Hardening Soil material model. The HS-model uses a linear Morh Coulumb yield criterion, in which the maximum shear stress of the material can be described by using the friction angle φ and the cohesion c. However, the ballast shear strength has been found to be a nonlinear stress-dependent quantity (Indraratna et al. 2011) and therefore the determination of the constant friction angle and cohesion term is not entirely unambiguous. The calculation parameters used for the ballast are based on the sources of Skoglund (2002), Suiker et al. (2005) Nurmikolu & Kolisoja (2010) Indraratna et al. (2011) and Kolos et al. (2017). Thus, it has been

Table 1. Material parameters used in FE modelling.

	y	E	E_oed	E_ur	v_ur	m	c'	ϕ	φ	R_f	K_0
	[kN/m^3]	*[MPa]*	*[MPa]*	*[MPa]*	*[-]*	*[-]*	*[kPa]*	*[°]*	*[°]*	*[-]*	*[-]*
Koria-Kouvola-model											
New ballast	17	420	420	840	0,2	0,65	5	53	18	0,5	0,35
Old ballast	18	400	365	800	0,2	0,7	4	50	17	0,5	0,35
Coarse sand	20	270	270	540	0,2	0,35	4	44,5	13	0,6	0,37
Gravel	19,5	475	475	950	0,2	0,5	3	51	17	0,55	0,35
Pori-Mäntyluoto-model											
Ballast layer	17	380	380	760	0,2	0,6	6	52	18	0,5	0,35
Fine sand	19,5	240	240	480	0,2	0,5	1	37	6	0,6	0,40

decided to use a friction angle of 50–53 ° and cohesion values of 4–6 kPa as the ballast layer strength parameters - other ballast parameters are listed in Table 1. The substructure calculation parameters of the Koria-Kouvola verification model are based on the laboratory test results reported by Kolisoja et al. (2000). In other respects, references Kolisoja (1997), Suiker et al. (2005) and Duncan et al. (2014) have been used to determine other parameters for the substructure layers. All calculation parameters are listed in Table 1.

4 TEST STRUCTURES AND VERIFICATION MODELS

Measurement data from two different test structures have been used to verify the calculation model. The first verification structure is in Eastern Finland on the double-track Koria-Kouvola line section. This test structure is characterized by a thick ballast layer with a total thickness of 1.2 meters, consisting of an upper 0.6-meter-thick new ballast layer and a lower 0.6-meter-thick old ballast layer. The total thickness of the test structure is 2.4 m, and the 1.2 m thick substructure consists of a 0.8 m thick layer of coarse-grained sand and a 0.4 m thick layer of gravel located on the surface of the subsoil. Sensors measuring vertical stress and strain are placed in the structure at different distances from the elevation line (el); el-0.7 m, el-1.3 m and el-2.0 m. Also, sensors measuring horizontal strains have been installed at heights el-0.7 m and el-1.3 m. The vertical displacements of the structure have been measured at three different points from the sleeper: at both ends and in the middle.

The second test structure is located in western Finland on the Pori-Mäntyluoto line section, a single-track section with a total thickness of 1.1 meters. The ballast layer of the structure is 0.5 meters thick, and the substructure consists of a 0.6-meter-thick fine-grained sand layer. Vertical, longitudinal, and transverse earth pressures have been measured below the sleeper from two different depths: from the upper part of the substructure layer (0.4 meters from the bottom of the sleeper) and from the lower part of the substructure layer (0.7 meters from the bottom of the sleeper) - a total of six different pressure sensors are installed in the substructure. Also, the vertical displacements of the structure have been measured from three different depths: from the top of the sleeper, elevation line -1.0 m and elevation line -1.5 m.

The geometry of the verification models is shown in Figure 1. The total length of the Koria-Kouvola calculation model is 36.8 meters, whereas the Pori-Mäntyluoto model is 48.8 meters long. The total width of both models is 30 meters, and the external load consists of three wagons. The thickness of the subsoil of the Koria-Kouvola verification model is 5 meters and its modulus of elasticity has a constant value of 56 MPa, while subsoil-layer Poisson's ration is 0.2. In the Pori-Mäntyluoto verification model, the subsoil is divided into two layers based on the Swedish weight sounding results; For a 2.2 m thick clay layer with an initial modulus of 50 MPa and a lower 3-meter-thick sand layer with an initial modulus of 100 MPa. The stiffness of the upper subsoil is assumed to increase linearly with respect to depth by 5 MPa per meter and the stiffness of the lower layer by 10 MPa per meter. A constant Poisson's ratio of 0.2 has been used for both subsoil layers.

Due to the lack of more accurate information, the loading diagram used in the Koria-Kouvola verification model used a bogie wheelbase spacing of 1.8 meters and a bogie spacing of 5.4 meters. The length of one train carriage in the calculation model is 10.8 meters, while the distance of the bogies of successive carriages is 1.8 meters. In turn, the test train at the Pori-Mäntyluoto site consisted of VOK-wagons with an axle weight of 20–22 tones (total wagon length 13.92 meters, bogie spacing 8.55 meters and bogie wheelbase 1.8 meters). A dense element mesh has been used in both models; the total number of elements in the Koria-Kouvola model is about 500,000 and, in the Pori-Mäntyluoto model about 350,000. A three-nobe beam elements have been used in the modeling of the rails and 10-nobe tetrahedral elements to modeling of the volume elements (more detailed mathematical description of the elements can be found in source Plaxis 2017 c).

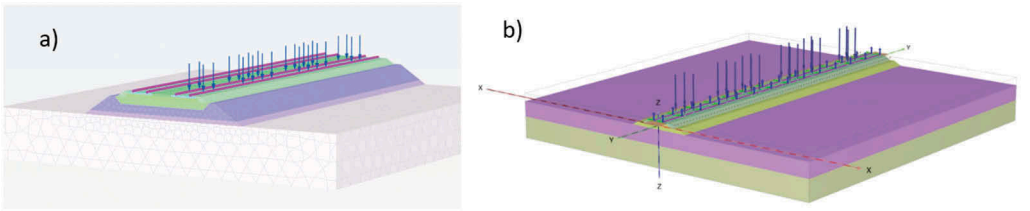

Figure 1. Koria-Kouvola FE-model (a) and Pori-Mäntyluoto FE-model (b).

5 VERIFICATION CALCULATIONS

5.1 *Koria-Kouvola*

Figure 2 shows the calculated and measured values of vertical stress increase, vertical and transverse strains, and vertical displacements of the sleeper under an axle load of 250 kN. According to the results, the modeling results seem to correspond to the behavior of the test structure very well. Only the calculated vertical stress level increase at a depth of 1.1 meters from the bottom of the sleeper is about 20% higher than the measured value. Correspondingly the model slightly underestimates the horizontal compression of the embankment material.

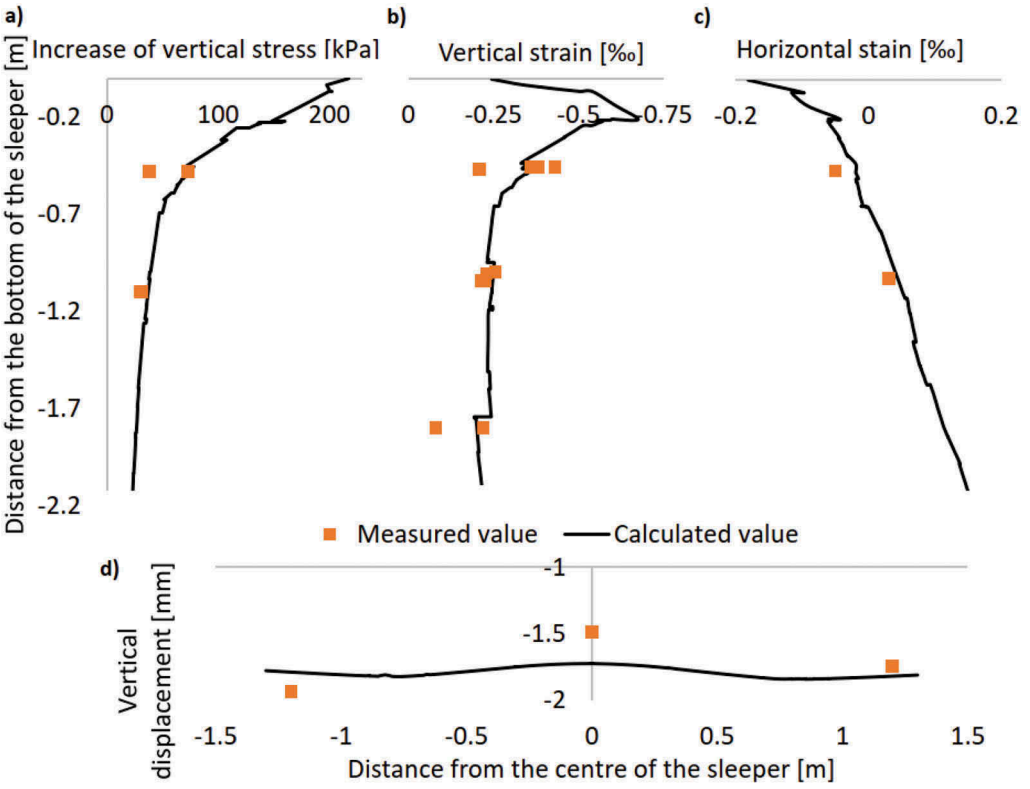

Figure 2. Measured and calculated vertical stress increments (a), vertical strains (b), horizontal strains (c) and vertical displacements of the sleeper (d).

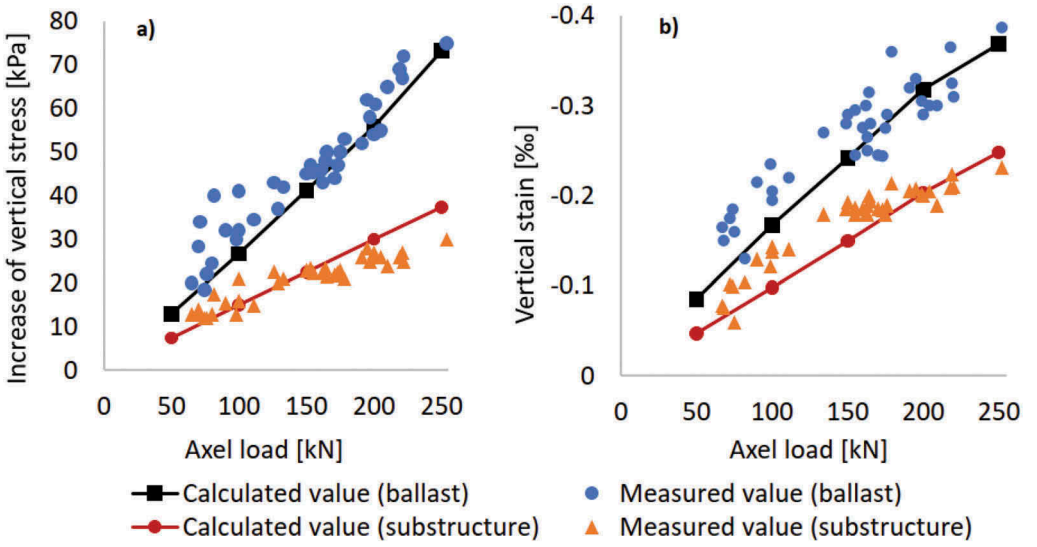

Figure 3. Measured and calculated vertical stress increases (a) and vertical strains (b) at different axel load levels.

Figure 3 shows the measured and calculated vertical stress and vertical strain levels at different axle loads at two different depths (el-0.7 m and el-1.3 m). At low load levels, the calculation model slightly underestimates the compression of the material, but in general the calculated values can be considered to correspond very well to the measured values - especially given the differences in load diagrams for vehicles with different axle loads.

As shown in Figure 3, the effect of axle load on the stress-strain response of the structure appears to be quite linear. For example, in the case of the Koria-Kouvola verification model, the vertical stress increase due to external axel load as a function of depth, can be described very accurately using the four-parameter approximation equation:

$$\sigma_{ZZ} = \frac{Q}{250}\left[\frac{180}{e^{\frac{z}{0,33}}} + \frac{43}{1+\frac{z}{2,29}}\right] \tag{3}$$

where Q is the axle load to be used (unit kN) and z is distance from the bottom of the sleeper (as meters). Equation 3 produces an excellent 0.9948 correlation with the modeling results (five different axle weight levels, 645 observation points). However, it should be noted that Equation 3 is intended to be used primarily on medium-rigid subgrades (E = 40 - 80 MPa) - on stiffer substrates it may underestimate the stress level of the structure. Also, if the load diagram significantly differs from the one used in the Koria-Kouvola model, the shape of the load distribution may slightly differ from the prediction of Equation 3.

5.2 *Pori-Mäntyluoto*

Figure 4 shows the measured and calculated vertical stress increments under the overrun of a test train with an axle weight of 208 kN. For the vertical stress increase in the upper substructure layer, the calculated and measured stress profiles are quite similar, but in the deeper structure, the calculation model slightly overestimates the stress increase under the bogie overrun. However, the measured and modeled longitudinal and transverse stress increment profiles in the lower substructure are very closely matched (Figure 5).

Figure 6 shows the measured and calculated vertical displacement profiles under the test train overrun. In general, the model corresponds very well to measured values of vertical displacements, especially the vertical displacements of the sleeper. Compared to the vertical displacement profile measured in the deeper structure, the calculation model slightly overestimates the structure displacement levels between the axles and the bogies, however, the magnitude of the maximum displacements under the axles is correct. In general, the calculated values can be found to correspond very well to the measurement results.

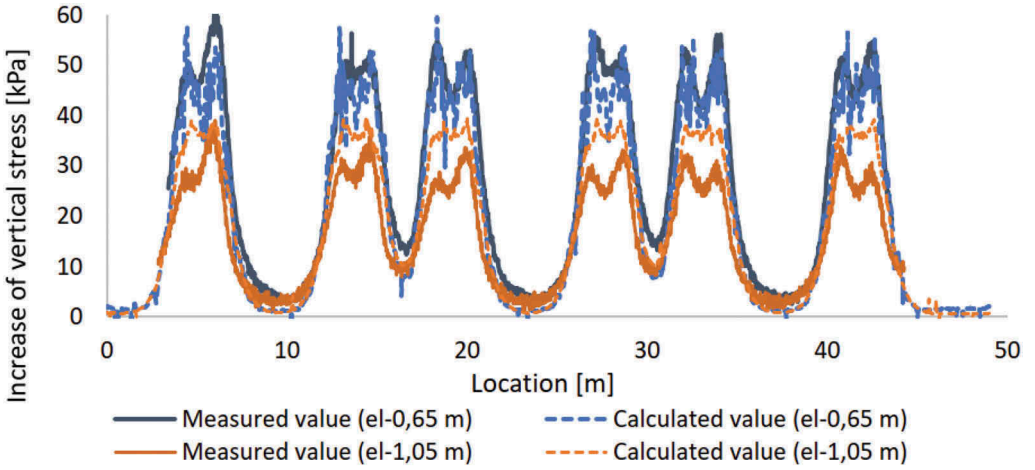

Figure 4. Calculated and measured vertical stress changes at two different depths (el-0.65 m and el-1.05 m).

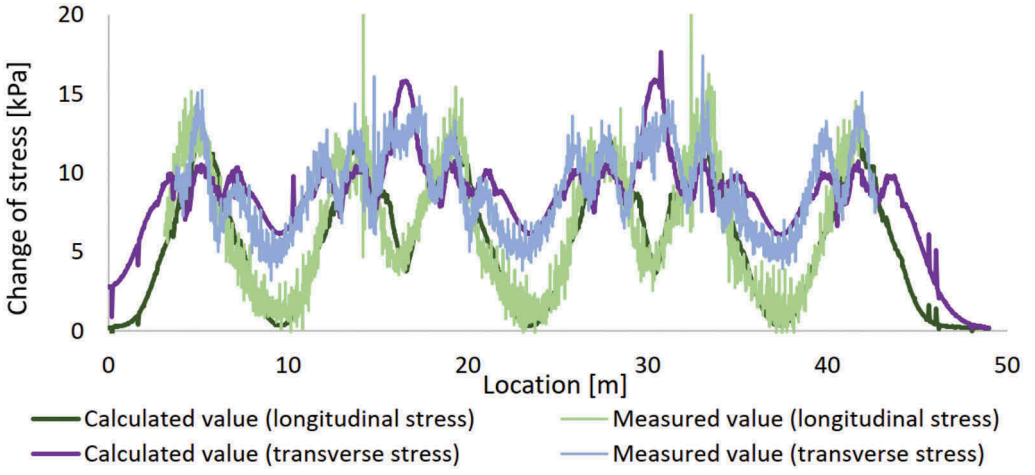

Figure 5. Calculated and measured longitudinal and transverse stress changes (at depth el-1.05 m).

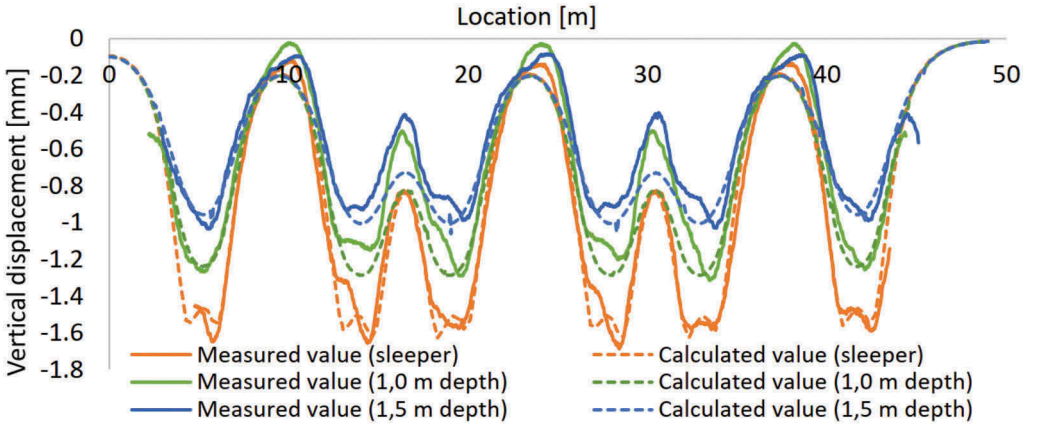

Figure 6. Measured and calculated vertical displacements at three different depths.

6 THE EFFECT OF SUBGRADE STIFFNESS

To illustrate the significance of subsoil conditions, a simulation series of six calculations was performed in which the modulus of subgrade stiffness was varied while its Poisson's ratio remained ration at 0.2. The two-meter substructure thickness and the material parameters of the Pori-Mäntyluoto verification model were used in the calculation. The subgrade consists of a single 5 m thick linear elastic layer with a constant modulus of elasticity. An axle load of 250 kN has been used in all calculations and the loading diagram is similar as in the Koria-Kouvola verification model.

Based on their miniature embankment experiments, carried out in laboratory conditions, Kalliainen & Kolisoja (2013) found that subgrade stiffness plays a key role in terms of the deterioration rate of the embankment geometry; when the deformations are large enough, the individual grains will no longer be able to return to their original position after the external loading has been removed. Figure 7a shows results on the computational effect of subgrade stiffness on the deformation level of the structure. When moving to flexible subgrades, the deformation level increases rapidly - especially in the upper part of the substructure. If the deviatoric strains are presented as a function of the vertical displacement of the sleeper, the trend is almost linear (Figure 7b). In flexible subgrades, deformations are typically large throughout the structure; when the subsoil deflects, the structure above must follow.

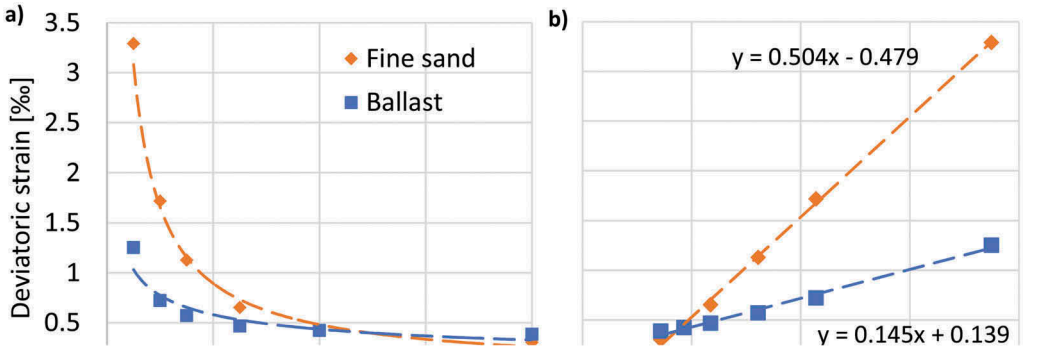

Figure 7. Deviator strains of the ballast layer and the upper part of the substructure as a function of subgrade stiffness (a) and as a function of vertical displacement of the sleeper (b).

7 CONCLUSIONS

1. In this study, a full-scale 3D computational model was created to examine the static stress-strain response of a railway structure using the finite element method. Comprehensive measurement data from two different test sites were used to verify the model, and data available from laboratory experiments were extensively utilized in the model parameterization. Based on the verification calculations performed, the calculation model corresponds very well in overall to the test structures in its behavior.
2. Based on calculations and field measurements, the effect of axle weight on the behavior of the structure appears to be quite linear. Based on the calculation results, a simple fitting model (Equation 3) was developed for estimating the stress level of the structure at different depths, producing an excellent correlation with the modeling results.
3. The subgrade stiffness seems to be the single most important factor in terms of the deviatoric strain levels of the structure - with flexible subgrades, the deformations are typically large throughout the structure. In practice, the strain levels of railway structure increase almost linearly as a function of subsoil deflection, which partly explains the relationship between the measured track stiffness and the rate of geometry deterioration.

ACKNOWLEDGMENTS

The authors gratefully acknowledge the Finnish Transport Infrastructure Agency for funding the study.

REFERENCES

Duncan J. M., Wriqht S. G., Brandon T. L. (2014). Soil strength and slope stability. John Wiley & Sons, Inc., Hoboken, New Jersey.

Gallego I., Muñoz J., Rivas A., Sánchez-Cambronero S. (2011). Vertical Track Stiffness as a New Parameter Involved in Designing High-Speed Railway Infrastructure. J. Transp. Eng., 2011, 137(12): 971–979.

Ganesh Babu K, Sujatha C (2010) Track modulus analysis of railway track system using finite element model. J Vib Control 16(10):1559–1574.

Hetényi, M. (1946). Beams on elastic foundation. Theory with applications in the fields of civil and mechanical engineering, The University of Michigan Press, Ann Arbor, 1946

Indraratna B., Nimbaikar S. (2013). Stress-strain degradation response of railway ballast stabilized with geosynthetics. J. Geotech. Geoenviron. Eng. 2013.139:684–700.

Indraratna B., Salim W., Rujikiatkamjorn C. (2011). Advanced Rail Geotechnology – Ballasted Track.

Kalliainen A & Kolisoja P. (2013). Modelling of the effect of embankment dimensions on the mechanical behaviour of railway track. (In Finnish) Finnish Transport Agency, Infrastructure and the Environment. Helsinki 2013. Research reports of the Finnish Transport Agency 33/2013. 85 pages and 2 appendices.

Kalliainen A, Kolisoja P, Nurmikolu A (2016) 3D finite element model as a tool for analysing the structural behaviour of a railway track. Procedia Eng 143:820–827

Kolisoja P. (1997). Resilient Deformation Characteristics of Granular Materials. Tampere University of Technology, Tampere.

Kolisoja P., Järvenpää I., Mäkelä E., Levomäki M. (2000) Instrumentation and Modelling of Track Structure, 250 kN and 300 kN axel loads. (In Finnish) Publications of Finnish Rail Administration. A5/2000. Finnish Rail Administration, Technical Unit. Helsinki 2000. 137 pp. + 15 app.

Kolos A., Konon A., Chistyakov P. (2017). Change of ballast strength properties during particles abrasive wear. Transportation Geotechnics and Geoecology, TGG 2017, 17-19 May 2017, Saint Petersburg, Russia.

Nurmikolu A. & Kolisoja P. (2010). Effects of ballast cleaning on the properties of railway ballast. (In Finnish) Finnish Transport Agency, Railway Department. Helsinki 2010. Research reports of the Finnish Transport Agency 11/2010. 64 pages and 3 appendices.

Plaxis. (2017). Plaxis Material Models Manual.

Plaxis (2017 b). Plaxis 3D Reference Manual.

Plaxis (2017 c). Plaxis Scientific Manual.
Powrie W, Yang L, Clayton CR (2007) Stress changes in the ground below ballasted railway track during train passage. Proc Inst Mech Eng Part F J Rail Rapid Transit 221(2):247–262.
Robnett, Q.L., Thompsom, M.R., Knutson, R.M. & Tayabji, S.D. (1975). Development of a structural model and materials evaluation procedures. Ballast and Foundation Materials Research Program, University of Illinois, report to FRA of US/DOT, Report No. DOT-FR.30038, May.
Sayeed A. (2016). Design of Ballasted Railway Track Foundations using Numerical Modelling with Special Reference to High Speed Trains. PhD thesis of Curtin University, Department of Civil Engineering.
Selig, E. T. & Waters, J. M. (1994). Track geotechnology and substructure management. London, Thomas Telford Publications. 407 p.
SFS-EN 13674-1:2011 + A1:2017 (2017). Railway applications. Track. Rail. Part 1: Vignole railway rails 46 kg/m and above.
Shahraki M., Salehi M., Witt K. J., Meier T. (2014). 3D Modelling of Train Induced Moving Loads on an Embankment. Plaxis Bulletin, Autumn issue 2014.
Skoglund K. A. (2002). A Study of Some Factors in Mechanistic Railway Track Design. Phd-thesis. Department of Road and Railway Engineering, Norwegian University of Science and Technology NTNU, Trondheim.
Sowmiya, L.S. Shahu, J.T. Gupta, K.K. (2010). Three-Dimensional Finite Element Analysis of Railway Track. Indian Geotechnical Conference – 2010, GEOtrendz December 16 –18, 2010.
Suiker, A. S. J., Selig, E. T., and Frenkel, R. (2005). "Static and cyclic triaxial testing of ballast and subballast." J. Geotech. Geoenviron. Engng., 131(6),771–782.
Varandas J. N., Paixão A., Fortunato E., Hölscher P. (2016). A Numerical Study on the Stress Changes in the Ballast due to Train Passages. Advances in Transportation Geotechnics 3. The 3rd International Conference on Transportation Geotechnics (ICTG 2016). 143: 1169–1176.
Winkler, e. (1867). Die lehere vonder Elastizität und Festikeit: Verlag H.Dominicus 1867.